Control of morphology and surface wettability of anodic niobium oxide microcones formed in hot phosphate-glycerol electrolytes

Shu Yang,[a] Hiroki Habazaki,*[a] Takashi Fujii,[a] Yoshitaka Aoki,[a] Peter Skeldon[b] and George E. Thompson[b]

[a] Division of Materials Chemistry, Faculty of Engineering, Hokkaido University, Sapporo, Hokkaido 060-8628, Japan.

[b] Corrosion and Protection Centre, School of Materials, The University of Manchester, Manchester M13 9PL, UK

Corresponding author: Fax: +81 11 706 6575; Tel:+81 11 706 6575;

E-mail:habazaki@eng.hokudai.ac.jp

Abstract

We report the fabrication of superhydrophobic surfaces with a hierarchical morphology by self-organized anodizing process. Simply by anodizing of niobium metal in hot phosphate-glycerol electrolyte, niobium oxide microcones, consisting of highly-branched oxide nanofibers, develop on the surface. The size of the microcones and their tip angles are controlled by changing the applied potential difference in anodizing and the water content in the electrolyte. Reduction of the water content increases the size of the microcones, with the nanofibers changing to nanoparticles. The size of microcones is also reduced by increasing the applied potential difference, without influencing the tip angle. The hierarchical oxide surfaces are superhydrophilic, with static contact angles close to 0^{o}. Coating of the anodic oxide films with a monolayer of fluoroalkyl phosphate makes the surfaces superhydrophobic with a contact angle for water as high as 175^{o} and a very small contact angle hysteresis of only 2^{o}. The present results indicate that the larger microcones with smaller tip angles show the higher contact angle for water.

Keywords: anodizing, nanoporous oxide, hierarchical surface, superhydrophobicity

1. Introduction

Superhydrophobic surfaces have received enormous attention in the past several years [1-4]. There are many important industrial applications of superhydrophobic surfaces, including self-cleaning windows and walls, anti-sticking of snow and anticorrosion of metals and microfluidics.

It is well known that wettability of solid surfaces is controlled by two factors: chemical composition and surface roughness [5]. In particular, to create a superhydrophobic surface that shows a static contact angle (CA) of greater than 150^o, with a small contact angle hysteresis (CAH) between advancing and receding contact angles, introduction of surface roughness is essential, since the maximum contact angle on a flat hydrophobic surface is ~120^o [6].

Roughness increases the solid-liquid contact area, which results in a high CA (θ), in accord with the Wenzel equation [7]:

$$\cos \theta = R_f \cos \theta_0 \qquad (1)$$

where θ_0 is the CA for smooth surface and R_f is the roughness factor. This equation reveals that the CA can increase due to roughness only when the surface is hydrophobic with $\theta_0 > 90^o$. For superhydrophobicity, the CAH must also be reduced. A composite solid-liquid-air interface should be formed with air pockets trapped in the cavities of the rough surface. The composite interface decreases dramatically the solid-liquid contact area, such that adhesion of

liquid to solid and the CAH decrease, allowing the water droplet to roll easily along the solid surface. The CA of liquid on the solid surface with air pockets is given by the Cassie-Baxter equation [8]:

$$\cos\theta = f_{ST}(\cos\theta_0 + 1) - 1 \qquad (2)$$

where f_{SL} is the fraction of solid in contact with liquid.

The composite interface with air pockets trapped in the cavities is a metastable state; an irreversible transition from the composite interface to the stable homogeneous interface, without air pockets by liquid filling the cavities, can occur, destroying the superhydrophobic properties [9]. It is now well accepted that hierarchical surface geometries are important to create and stabilize the composite interface for superhydrophobicity. In fact, many superhydrophobic surfaces that occur in nature, such as on lotus leaves, water strider legs and cicada wings, have hierarchical, multi-scale roughness on their surfaces [4]. Nosonovsky demonstrated recently that the introduction of nano-convex surfaces on micrometer-pillars prevents water droplets from penetrating into the cavities between the pillars, due to pinning effect [10].

Here we report the fabrication of self-organized hierarchical surfaces by simple anodizing. Anodizing of metals is one of the typical self-organizing processes that is used to form nanoporous oxide films, with ordered arrays of cylindrical pores. For aluminium, porous oxide films with hexagonally-ordered pore arrays are developed by anodizing in acid

electrolytes [11-13]. The fabrication of self-organized porous anodic oxides has been extended to other metals since the report of self-organized anodic TiO_2 in 1999 [14]. Extensive studies have been carried out recently on self-organized anodic TiO_2 nanotubes formed in fluoride-containing aqueous and organic electrolytes, due to their widespread potential uses, including photocatalysis, sensors, self-cleaning, dye-sensitized solar cells, and biomedical applications [15-17]. Self-organized porous anodic oxides have also been formed on zirconium [18], niobium [19], tantalum [20], and even on iron [21-23].

Besides aluminium, nanoporous or nanotubular anodic oxide films on valve metals have been developed mostly in the fluoride-containing aqueous and organic electrolytes. A new hot phosphate-glycerol electrolyte was first used in 1998, resulting in non-thickness-limited growth of barrier-type anodic oxide films on valve metals [24]. Later, it was found that the anodic films formed in the electrolyte were of a porous type, and their pore sizes were generally very small, 10 nm or less [25-27].

Self-organized, porous anodic oxides generally contain pores of a single size. Some of the authors found recently that microcones of anodic niobium oxide that consist of branched nanofibers developed in the hot phosphate-glycerol electrolyte [28, 29]. The formation of the microcones is associated with crystallization of the anodic oxide, which occurs during anodizing. The crystal growth at the metal/film interface leads to a conical shape, and simultaneous preferential dissolution of the initially-formed amorphous oxide discloses the

microcones after prolonged anodizing [28]. Using hierarchical microcone-nanofiber surface, superhydrophobic surface with a static CA of 158º was obtained after coating with a monolayer of fluoroalkylsilane. In this study we examined the change in the morphology of microcones with the water concentration in electrolyte and applied potential difference in anodizing. We report in this study extremely high CA of ~175º and CAH as small as 2º at the optimized morphology of the niobium oxide microcones coated with a fluoroalkyl phosphate layer. Such surfaces with extremely high CA (170 – 180º) are interesting, but only limited examples have been reported [30-33].

2. Experimental

High purity (99.9 mass%) niobium sheets of 0.2 mm thickness were used to form anodic oxide films. The niobium sheets, after coating with silicone to define a working area of 6 cm^2, were anodized at selected applied potential differences between 10 V and 15 V in stirred glycerol electrolyte containing 0.6 mol dm^{-3} K_2HPO_4 and 0.2 mol dm^{-3} K_3PO_4 at 443 K for 5.4 ks in a dry nitrogen atmosphere. The water content in the electrolyte was controlled to 0.1, 0.25 or 0.5 mass%, as measured by the Karl-Fisher titration method before anodizing. The electrolyte was contained in a separable glass flask, which was heated to selected temperatures by a heating mantle. A two-electrode cell with a platinum counter electrode was used. A constant current density of 250 A m^{-2} was applied before reaching the selected

potential difference. During anodizing, the potential differnce and current were recorded on a PC through an Advantest, 7352A digital multimeter.

After anodizing, the surfaces and fractured cross-sections of the specimens were observed in a JEOL JSM-6500F field emission gun scanning electron microscope operated at 10 kV. Furthermore, the structure of some of the specimens was examined using a JEOL, JEM-2000FX transmission electron microscope operated at 200 kV. Electron-transparent sections were prepared using a Hitachi, FB-2100 focused ion beam system. The structure of the anodic films was also identified by X-ray diffraction (XRD) using Cu Kα radiation. A Rigaku, RINT-2000 system was used to record the XRD patterns.

The oxide surface following anodizing was hydrophilic. In order to make the surface hydrophobic, the anodized specimens were immersed in an ethanol solution containing 2 mass% FAP (fluoroalkyl phosphate, $CF_3(CF_2)_7CH_2CH_2OPO(OH)_2$) for more than 5 days to coat the oxide surfaces with a monolayer of FAP. Dynamic advancing and receding contact angles of the coated and non-coated specimens for water droplet were recorded using a Kyowa Interface Science, DM-CE1 optical contact angle meter. For the measurements, water was pumped into/sucked from the drop with a syringe. The transient behaviour of the contact angle was recorded and found to plateau as the advancing/receding value was reached. Each angle, determined using ellipse fitting mode, was measured multiple times, resulting in an average value with a standard deviation of ~1º. For the measurements, water droplets around

2 μL were used.

3. Results and discussion

3.1. Formation of Anodic Niobium Oxide Microcones

Figure 1a shows the current-time and potential difference-time responses during anodizing of niobium at 10 V in glycerol electrolyte containing 0.6 mol dm^{-3} K_2HPO_4 and 0.2 mol dm^{-3} K_3PO_4 with three different concentrations of water at 443 K. The anodizing time to reach 10 V is delayed by reducing the water concentration, from 150 s at 0.5 mass% water to 400 s at 0.1 mass% water. The current during anodizing at 10 V increases with decreasing water concentration in the electrolyte, and reveals a peak in the early stage of anodizing, which is associated with crystallization of anodic oxide [29, 34]. In Fig. 1a the current peak is not as obvious at a water concentration of 0.1 mass%, due to the reduced nucleation density of crystalline oxide, as discussed later.

Figure 1b shows the influence of applied potential difference in the electrolyte containing 0.25 mass% water. The final current density after anodizing for 5.4 ks is similar at all applied potential differences, but the current peak appears at shorter time and the peak current density increases with an increase in the applied potential difference. The results suggest that the nucleation and growth of crystalline oxide are accelerated by increasing the applied potential difference.

Figure 2 shows SEM images of the surfaces (Figs. 2a-c) and cross-sections (Figs. 2d-f) of the anodic oxide films formed at 10 V in the electrolytes with different water concentrations. At all water concentrations, anodic oxide microcones are formed as clearly seen from the cross-sectional images (Figs. 2d-f). The formation of the microcones is associated with crystallization of anodic oxide in a barrier layer between an outer porous layer and metal substrate during anodizing and preferential dissolution of an initially formed, outer amorphous oxide layer [29]. It appears from surface images that entire surfaces are covered with microcones, although initially formed amorphous oxide, indicated using arrows in Fig. 2a, remains partly at 0.1 mass% water. The size of the microcones decreases with an increase in the water concentration, from 10-90 μm at 0.1 mass% water to 1-5 μm at 0.5 mass% water. In addition to the change in the size of microcones, the tip angle of the microcones changes with water concentration, from ~110° at 0.1 mass% water to ~60° at 0.5 mass% water (Figs. 2d-f). The total film thickness reduced with increasing the water concentration, in agreement with the reduction of current density shown in Fig. 1a.

The microcones consist of highly branched nanofibers at water concentrations of 0.25 and 0.5 mass% (Figs. 3b-c), in agreement with the previous reports [28, 29]. However, such fibrous morphology is not obvious and a nanoparticle-like feature is found in the high magnification surface images of the microcones formed at 0.1 mass% water (Fig. 3a).

The applied potential difference also changes the size of microcones. Fig. 4 shows SEM

images of the surfaces of the anodic oxide films formed at 12 V (Fig, 4a) and 15 V (Fig. 4b) in the electrolyte containing 0.25 mass% water. From the comparison also with Fig. 2b, showing the anodic film formed at 10 V, it can be said that the microcones become smaller with increasing the applied potential difference. The size is mostly less than 3 μm at 15 V. Although the size of microcones changes with the applied potential difference, all the microcones formed at 10 to 15 V in the electrolyte containing 0.25 mass% water have similar tip angles of ~90°, as shown in Fig. 2e and Fig. 5. Thus, the tip angle is only dependent upon the water concentration, not upon the applied potential difference.

Figure 6 shows XRD patterns of the niobium specimens anodized at 10 V in the electrolytes with different water concentrations (Fig. 6a) and at three different applied potential differences in the electrolyte with 0.25 mass% water (Fig. 6b). Regardless of the water concentrations in the electrolyte and the applied potential differences examined, similar XRD patterns with peaks of crystalline Nb_2O_5 (JCPDS 30-873) and the niobium substrate were obtained. Thus, despite the changes in the size and tip angle of anodic oxide microcones, the same crystalline oxide is formed at different water concentrations and at different applied potential differences.

Cross-sections of the anodic oxide films were examined also by transmission electron microscopy. Fig. 7 shows an example of the anodic oxide film formed at 10 V in the electrolyte containing 0.25 mass% water. Only the film region close to the niobium substrate

is revealed in this figure. Although branched fibrous morphology is observed on the surface (Fig. 3b), many cylindrical nanopore channels, which are all approximately normal to the metal/film interface, are developed. Such pore channels resemble those in usual porous anodic alumina films formed in aqueous acid electrolytes [12]. The diameter of the cylindrical pores is apparently ~10 nm or less. The pores do not penetrate to the substrate and a non-porous layer, ~35 nm thick, referred as to a barrier layer, is present between the porous layer and the metal substrate.

3.2. Superhydrophobicity of Anodic Niobium Oxide Microcones

Since the size and tip angle of the anodic niobium oxide microcones could be changed by anodizing conditions, surface wettability of the microcone surfaces were examined. All the niobium oxide microcone surfaces produced were superhydrophilic with a CA for a water droplet close to 0°. To make the oxide surface hydrophobic, the anodized specimens were coated with FAP, which was selected for two main reasons. One is that CF_3-terminal group is the most effective in reducing the surface energy [6] and another is that the fluoroalkyl phosphate is known to bring about higher CAs for water and oil rather than the often used fluoroalkylsilane coupling agents [35]. The FAP-coated anodic niobium oxide films were superhydrophobic, and the static CA for water could not be measured, because of the ready rolling of the water droplet from the surface. Thus, dynamic CAs were measured by an

extension/contraction method. As expected from the rolling of the droplet on the surface, the difference between the advancing and receding CAs, i.e. the CAH, is very small, being only 3°, as shown in Fig. 8. The coated microcones surface formed at 10 V in 0.5 mass% water shows an advancing CA as high as 175º. The change in the advancing and receding CAs with the water concentration in the electrolyte used to form the microcones (Fig. 9a) reveals enhanced contact angles at higher water concentrations. Even at the lower water concentration of 0.1 mass%, the CAH is only 2° and the receding contact angle is more than 165°. Such results indicate the suitability of the self-organized, hierarchical microcones surfaces, consisting of branched nanofibers, for fabrication of superhydrophobic surfaces.

When the water concentration is changed at an applied potential difference of 10 V, both the size and tip angle of the microcones change. In contrast, only the size of microcones depends on the applied potential difference, with the tip angle of microcones being a constant value of ~90°. Thus, the influence of the size of microcones on CA is examined. As shown in Fig. 9b, the CA decreases with an increase in the applied potential difference, i.e. with a decrease in the size of microcones. From a comparison between the results shown in Figs. 9a and 9b, it can be said that the microcones with larger size and smaller tip angle are preferable to enhance the CA for water.

4. Discussion

It was found in the previous study that an amorphous nanoporous anodic oxide film was initially formed [28]. During anodizing crystalline oxide nucleated at the barrier layer located between the porous layer and the metal substrate and grew in a conical shape. Chemical dissolution of the initially formed amorphous oxide proceeded during anodizing and then, microcone-shaped, chemically more stable crystalline oxide appeared on the surface after prolonged anodizing. The nucleation of the crystalline oxide should be initiated before a current peak observed in Fig. 1. To confirm the formation of crystalline oxide at the current peak region, anodizing of niobium only for 900 s was carried out at 10 V in 0.25 mass% water. The surface of the as-anodized specimen was covered with the nanoporous amorphous oxide layer, but simply after immersion in the electrolyte for 1.8 ks, microcone-shaped oxide, which should be crystalline, appeared on the surface as a consequence of preferential dissolution of the amorphous oxide that covered the microcones (Fig. 10a). At this anodizing time the substrate surface is not entirely covered with the microcones and some small microcones are isolated. Even at this stage, the microcone consists of branched nanofibers, as seen in the high magnification image of Fig. 10b.

Crystallization of amorphous anodic oxides was reported to occur also during growth of barrier-type anodic oxide films on niobium and tantalum in aqueous electrolytes [36, 37]. In the field-induced crystallization of barrier-type anodic niobium oxide, the crystalline niobium oxide thickened faster than the amorphous niobium oxide under the high electric field [34],

suggesting lower ionic resistivity of the crystalline oxide. A current peak appeared when field-induced crystallization occurred during growth of barrier-type anodic oxide films [36, 37]. Since similar current peak is observed in the present study (Fig. 1), it is likely that the crystalline oxide formed in the present anodic oxide films also has lower ionic resistivity, and hence increases the current.

After the current peak, the current decreases continuously (Fig. 1). During growth of porous anodic oxide films, the thickness of the barrier layer is generally unchanged at a constant applied potential difference at steady state [12]. Thus, usually, a steady-state current is observed during growth of porous anodic oxide films. However, continuous current decay was reported for porous film growth on aluminum under hard anodizing conditions, i.e., at high applied potential differences, and explained in terms of the film growth controlled by a diffusion-limited process [38]. Similar to the hard anodizing of aluminum, probably the extension of diffusion path developed in the nanopores from the pore base reduces the current during anodizing, as discussed in a previous paper [39].

For the barrier-type film growth on tantalum, nucleation of crystalline oxide was accelerated at higher applied potential differences [40]. From the nucleation sites the crystalline area expanded radially during further anodizing [40]. Since the high electric field is applied only in the barrier layer beneath the porous layer in the present porous anodic oxide films, the field-induced crystallization occurs only in the barrier layer. The radial growth of crystalline

oxide in the barrier layer produces a conical crystalline region. The nucleation density of crystalline oxide increases with an increase in the applied potential difference. Thus, at higher applied potential differences the surface is covered by a larger number of small microcones. Due to the enhancement of the nucleation, the current peak appears at shorter anodizing time at higher applied potential differences (Fig. 1b).

Although the size of microcones changes with the applied potential difference, all the microcones formed at 10 to 15 V in the electrolyte containing 0.25 mass% water have similar tip angles of ~90°, as shown in Fig. 2e and Fig. 5. The tip angle is dependent only upon the water concentration (Fig. 2), not upon the applied potential difference. The tip angle may be controlled by the ratio of the radial growth rate of crystalline oxide in the barrier layer to the growth rate of porous anodic oxide film. The increase in the ratio may increase the tip angle. The findings in the present study suggest that the nucleation of crystalline oxide is accelerated by the addition of water, but the radial growth rate is enhanced by reducing the water concentration. Thus, smaller microcones with smaller tip angles form at higher water concentrations.

The electric field strength applied in the barrier layer during film growth may influence the growth of crystalline oxide. The field strength decreases with water concentration when a porous anodic oxide films are grown on niobium in hot glycerol electrolyte containing 0.8 mol dm^{-3} K_2HPO_4 [27]. In order to examine the influence of water concentration on the field

strength in the case of the present electrolyte containing both K_2HPO_4 and K_3PO_4, re-anodizing experiments were carried out. The specimens anodized in the present electrolytes with different water concentrations were re-anodized in aqueous buffer electrolyte containing 0.5 mol dm^{-3} H_3BO_3 and 0.05 mol dm^{-3} $Na_2B_4O_7$ (pH 8.4), in which a barrier-type anodic oxide film grew at high current efficiency. An initial potential difference surge should be observed during re-anodizing, which is proportional to the thickness of the barrier layer [41]. Table 1 shows the change in the initial surge cell potential difference for the specimens anodized at 10 V in the electrolytes with different water concentrations. The surge cell potential differnce increases with increasing water concentration, such that a thicker barrier layer is formed at a higher water concentration. This finding is in agreement with the higher current density at lower water concentration (Fig. 1a). The increase in current density by reducing the water concentration is associated with an enhanced field in the barrier layer during film growth. The higher field strength may accelerate the radial growth of the crystalline oxide greater than the thickening of the anodic oxide film, leading to the larger tip angles at lower water concentrations. The growth process of the crystalline niobium oxide microcones at different water concentrations is illustrated in Fig. 11.

After FAP coating, the microcones surfaces are superhydrophobic. The CA becomes larger with increasing the size of microcones and reducing their tip angle. Because of the small CAH of 2-3º for the FAP-coated microcones, the Cassie-Baxter state with air pockets between water

droplet and the microcones surface must be established. The change in the CA with the size of microcones and their tip angle appears to follow the Eq. 2, since the fraction of solid in contact with water droplet should be lower for the larger microcones and those with smaller tip angles.

5. Conclusions

In summary, the present study reveals the fabrication of self-organized, hierarchical oxide surfaces on niobium by a simple anodizing technique. After coating the hierarchical surfaces with a fluoroalkylphosphate layer to reduce the surface energy, the surfaces become superhydrophobic with an extremely high CA close to 175° and a small contact angle hysteresis of only ~2°. The anodizing in hot phosphate-glycerol electrolyte leads to the formation of porous niobium oxide microcones, which consist of highly branched nanofibres. The formation of self-organized niobium oxide microcones is associated with crystallization of anodic oxide during anodizing and preferential dissolution of an initially-formed, amorphous oxide layer. The size of microcones is controlled by the water concentration in the electrolyte as well as applied potential difference, but the tip angle of microcones is only influenced by the water concentration. Water repellency tends to be enhanced by reducing the tip angle and increasing the size of the microcones.

Acknowledgments

The present work is supported in part by a Grant-in-Aid for Exploratory Research, No.21656180 from the Japan Society for the Promotion of Science, and also by the Global COE Program (Project No. B01: Catalysis as the Basis for Innovation in Materials Science) from the Ministry of Education, Culture, Sports, Science and Technology, Japan.

References

[1] T.L. Sun, L. Feng, X.F. Gao, L. Jiang, Acc. Chem. Res., 38 (2005) 644-652.

[2] X.J. Feng, L. Jiang, Adv. Mater., 18 (2006) 3063-3078.

[3] M. Nosonovsky, B. Bhushan, Curr. Opin. Colloid Interface Sci., 14 (2009) 270-280.

[4] B. Bhushan, Y.C. Jung, Prog. Mater. Sci., 56 (2011) 1-108.

[5] N.J. Shirtcliffe, G. McHale, S. Atherton, M.I. Newton, Adv. Colloid Interface Sci., 161 (2010) 124-138.

[6] T. Nishino, M. Meguro, K. Nakamae, M. Matsushita, Y. Ueda, Langmuir, 15 (1999) 4321-4323.

[7] R.N. Wenzel, Ind. Eng. Chem., 28 (1936) 988-994.

[8] A.B.D. Cassie, S. Baxter, Trans. Faraday Soc., 40 (1944) 546-551.

[9] D. Quere, Rep. Prog. Phys., 68 (2005) 2495-2532.

[10] M. Nosonovsky, Langmuir, 23 (2007) 3157-3161.

[11] F. Keller, M.S. Hunter, D.L. Robinson, J. Electrochem. Soc., 100 (1953) 411.

[12] J.P. O'Sullivan, G.C. Wood, Proc. R. Soc. London, A, 317 (1970) 511-543.

[13] G.E. Thompson, Thin Solid Films, 297 (1997) 192-201.

[14] V. Zwilling, E. Darque-Ceretti, A. Boutry-Forveille, D. David, M.Y. Perrin, M. Aucouturier, Surf. Interface Anal., 27 (1999) 629-637.

[15] G.K. Mor, O.K. Varghese, M. Paulose, K. Shankar, C.A. Grimes, Sol. Energy Mater., 90 (2006) 2011-2075.

[16] J.M. Macak, H. Tsuchiya, A. Ghicov, K. Yasuda, R. Hahn, S. Bauer, P. Schmuki, Curr. Opin. Solid State Mater. Sci., 11 (2007) 3-18.

[17] A. Ghicov, P. Schmuki, Chem. Commun., (2009) 2791-2808.

[18] H. Tsuchiya, J.M. Macak, A. Ghicov, L. Taveira, P. Schmuki, Corros. Sci., 47 (2005) 3324-3335.

[19] J.S. Choi, J.H. Lim, S.C. Lee, J.H. Chang, K.J. Kim, M.A. Cho, Electrochim. Acta, 51 (2006) 5502-5507.

[20] I.V. Sieber, P. Schmuki, J. Electrochem. Soc., 152 (2005) C639-C644.

[21] H. Habazaki, Y. Konno, Y. Aoki, P. Skeldon, G.E. Thompson, J. Phys. Chem. C, 114 (2010) 18853-18859.

[22] R.R. Rangaraju, A. Panday, K.S. Raja, M. Misra, J. Phys. D: Appl. Phys., 42 (2009) 135303.

[23] R.R. Rangaraju, K.S. Raja, A. Panday, M. Misra, Electrochim. Acta, 55 (2010) 785-793.

[24] B. Melody, T. Kinard, P. Lessner, Electrochem. Solid State Let., 1 (1998) 126-129.

[25] Q. Lu, G. Alcala, P. Skeldon, G.E. Thompson, M.J. Graham, D. Masheder, K. Shimizu, H. Habazaki, Electrochim. Acta, 48 (2002) 37-42.

[26] Q. Lu, T. Hashimoto, P. Skeldon, G.E. Thompson, H. Habazaki, K. Shimizu, Electrochem. Solid State Let., 8 (2005) B17-B20.

[27] H. Habazaki, Y. Oikawa, K. Fushimi, Y. Aoki, K. Shimizu, P. Skeldon, G.E. Thompson, Electrochim. Acta, 54 (2009) 946-951.

[28] Y. Oikawa, T. Minami, H. Mayama, K. Tsujii, K. Fushimi, Y. Aoki, P. Skeldon, G.E. Thompson, H. Habazaki, Acta Mater., 57 (2009) 3941-3946.

[29] S. Yang, Y. Aoki, H. Habazaki, Appl. Surf. Sci., 257 (2011) 8190-8195.

[30] T. Onda, S. Shibuichi, N. Satoh, K. Tsujii, Langmuir, 12 (1996) 2125-2127.

[31] E. Hosono, S. Fujihara, I. Honma, H.S. Zhou, J. Am. Chem. Soc., 127 (2005) 13458-13459.

[32] L.C. Gao, T.J. McCarthy, J. Am. Chem. Soc., 128 (2006) 9052-9053.

[33] I.A. Larmour, S.E.J. Bell, G.C. Saunders, Angew. Chem.-Int. Edit., 46 (2007) 1710-1712.

[34] H. Habazaki, T. Ogasawara, H. Konno, K. Shimizu, S. Nagata, P. Skeldon, G.E. Thompson, Corros. Sci., 49 (2007) 580-593.

[35] S. Shibuichi, T. Yamamoto, T. Onda, K. Tsujii, J. Colloid Interface Sci., 208 (1998)

287-294.

[36] D.A. Vermilyea, J. Electrochem. Soc., 102 (1955) 207-214.

[37] K. Nagahara, M. Sakairi, H. Takahashi, K. Matsumoto, K. Takayama, Y. Oda, Electrochim. Acta, 52 (2007) 2134-2145.

[38] W. Lee, R. Ji, U. Gosele, K. Nielsch, Nat. Mater., 5 (2006) 741-747.

[39] Y. Oikawa, K. Fushimi, Y. Aoki, H. Habazaki, ECS Trans, 16 (2008) 345-351.

[40] D.A. Vermilyea, J. Electrochem. Soc., 104 (1957) 542-546.

[41] C. Wada, H. Asoh, S. Ono, Elechem., 73 (2005) 145-149.

Figure captions

Fig. 1 Current-time and cell potential differnce-time responses of niobium during anodizing in 0.6 mol dm^{-3} K_2HPO_4 and 0.2 mol dm^{-3} K_3PO_4-glycerol electrolytes at 443 K: a) at 10 V and different water concentrations of 0.1, 0.25 and 0.5 mass%; b) at different applied potential differences of 10, 12 and 15 V and water concentration of 0.25 mass%. The initial current density is 250 A m^{-2}.

Fig. 2 SEM surface (a-c) and cross-sectional (d-f) images of niobium after anodizing at 10 V in 0.6 mol dm^{-3} K_2HPO_4 and 0.2 mol dm^{-3} K_3PO_4-glycerol electrolytes containing (a, d) 0.1 mass%, (b, e) 0.25 mass% and (c, f) 0.5 mass% water at 443 K for 5.4 ks.

Fig. 3 High magnification SEM surface images of niobium after anodizing at 10 V in 0.6 mol dm^{-3} K_2HPO_4 and 0.2 mol dm^{-3} K_3PO_4-glycerol electrolytes containing (a) 0.1 mass%, (b) 0.25 mass% and (c) 0.5 mass% water at 443 K for 5.4 ks.

Fig. 4 SEM surface images of niobium after anodizing at (a) 12 V and (b) 15 V in 0.6 mol dm^{-3} K_2HPO_4 and 0.2 mol dm^{-3} K_3PO_4-glycerol electrolyte containing 0.25 mass% water at 443 K for 5.4 ks.

Fig. 5 SEM cross-sectional images of the anodic oxide films formed on niobium at (a) 12 V and (b) 15 V in 0.6 mol dm^{-3} K_2HPO_4 and 0.2 mol dm^{-3} K_3PO_4-glycerol electrolyte containing 0.25 mass% water at 443 K for 5.4 ks.

Fig. 6 X-ray diffraction patterns of niobium anodized in 0.6 mol dm^{-3} K_2HPO_4 and 0.2 mol dm^{-3} K_3PO_4-glycerol electrolytes at 443 K for 5.4 ks: a) at 10 V and different water concentrations of 0.1, 0.25 and 0.5 mass%; b) at different applied potential differences of 10, 12 and 15 V and water concentration of 0.25 mass%.

Fig. 7 TEM image of a FIB cross-section of the inner part of the anodic oxide film formed on niobium at 10 V in 0.6 mol dm^{-3} K_2HPO_4 and 0.2 mol dm^{-3} K_3PO_4-glycerol electrolyte containing 0.25 mass% water at 443 K for 5.4 ks.

Fig. 8 (a) Advancing and (b) receding CAs for water droplet on the niobium specimen anodized at 10 V in in 0.6 mol dm^{-3} K_2HPO_4 and 0.2 mol dm^{-3} K_3PO_4-glycerol electrolyte containing 0.5 mass% water at 443 K for 5.4 ks, and subsequently coated with FAP.

Fig. 9 Change in the advancing and receding contact angles for water with (a) the water concentration in the electrolyte at 10 V and (b) the applied potential difference at water concentration of 0.25 mass% for the formation of niobium oxide microcones.

Fig. 10 SEM surface images of niobium after anodizing at 10 V in 0.6 mol dm^{-3} K_2HPO_4 and 0.2 mol dm^{-3} K_3PO_4-glycerol electrolyte containing 0.25 mass% water at 443 K for 900 s and subsequent immersion in the electrolyte for 1.8 ks.

Fig. 11 Schematic illustration showing the formation process of anodic oxide microcones at different water concentrations.

Table 1 Surge cell potential differnces during re-anodizing of the niobium specimens at a constant current density of 5 Am^{-2} in 0.5 mol dm^{-3} H_3BO_3–0.05 mol dm^{-3} $Na_2B_4O_7$ aqueous solution at 293 K. The niobium specimens were prepared by anodizing at 10 V in 0.6 mol dm^{-3} K_2HPO_4 and 0.2 mol dm^{-3} K_3PO_4-glycerol electrolytes containing 0.1, 0.25 and 0.5 mass% water for 5.4 ks.

Water concentration (mass%)	0.1	0.25	0.5
Surge cell potential difference (V)	9.5	10.9	11.3

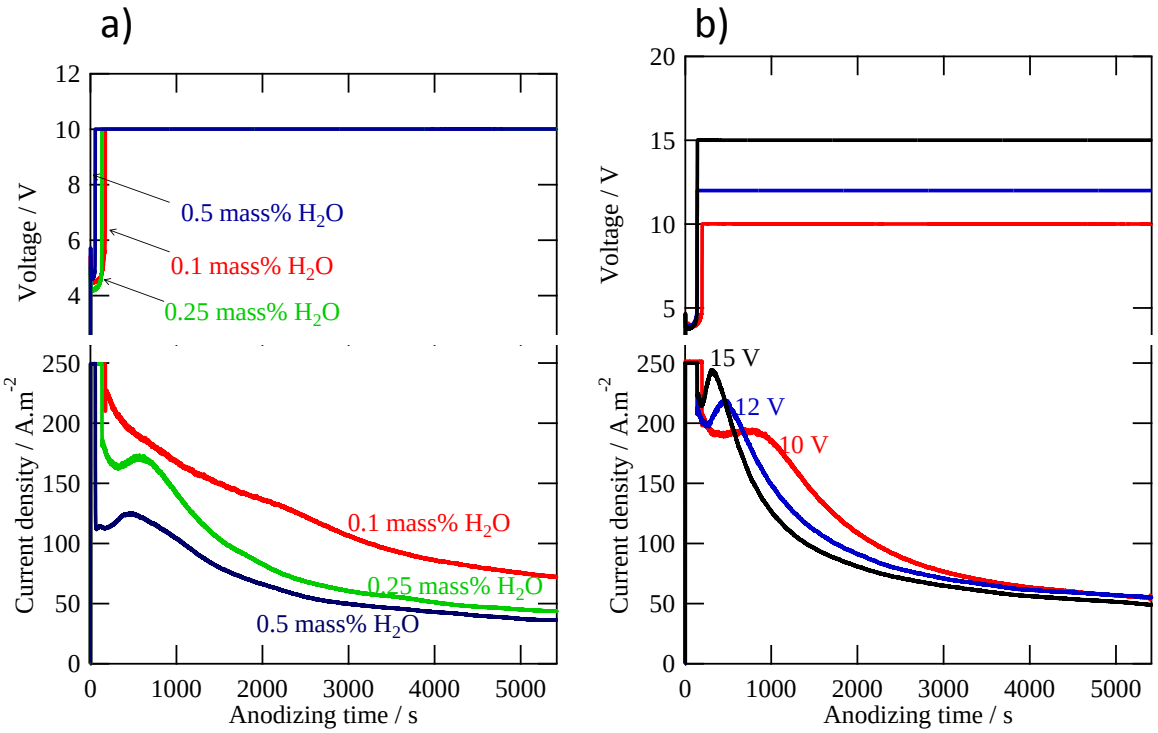
a)
b)
Voltage / V
Current density / A.m-2
Anodizing time / s
0.5 mass% H2O
0.1 mass% H2O
0.25 mass% H2O
15 V
12 V
10 V

Fig. 1

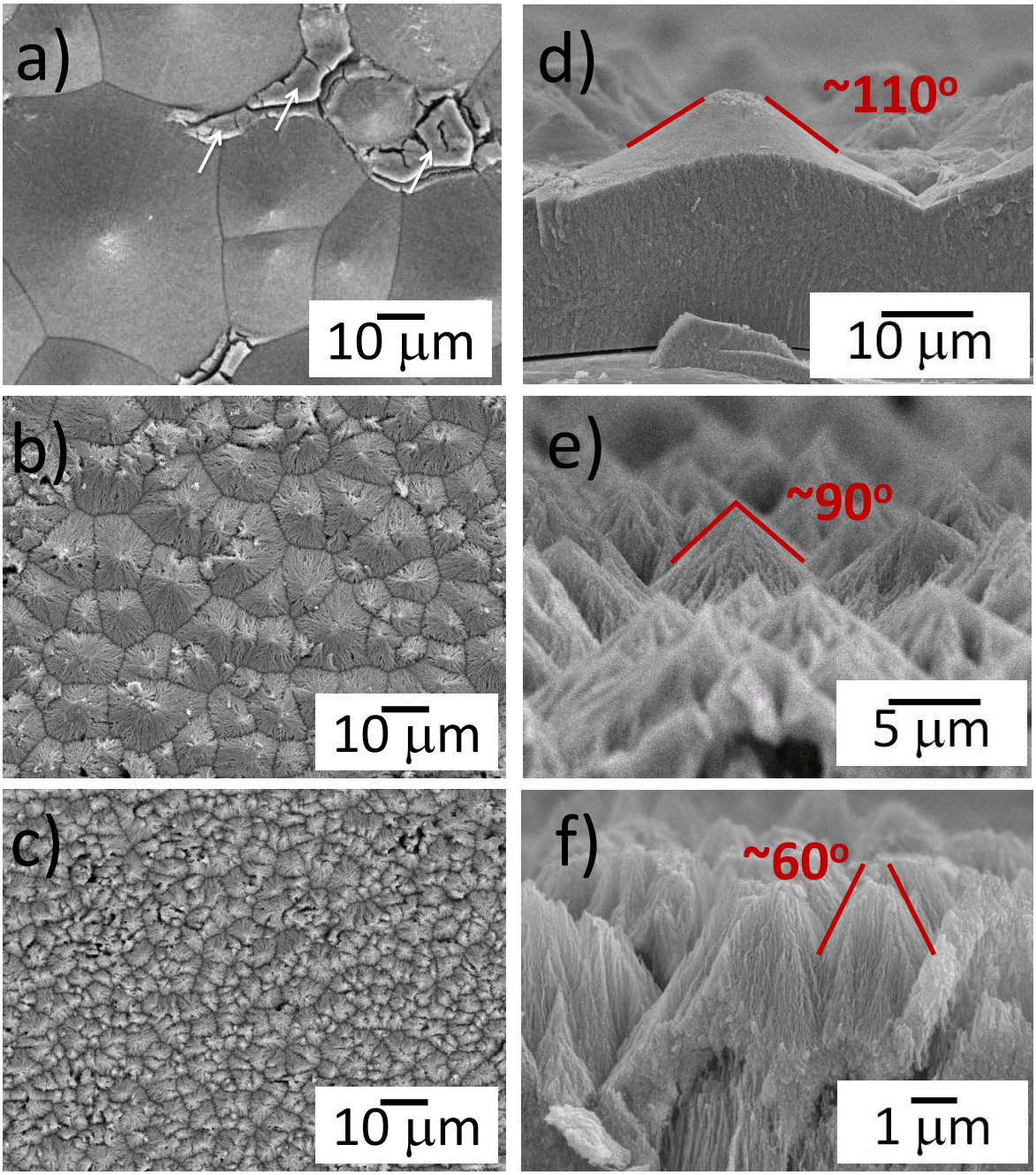

Fig. 2

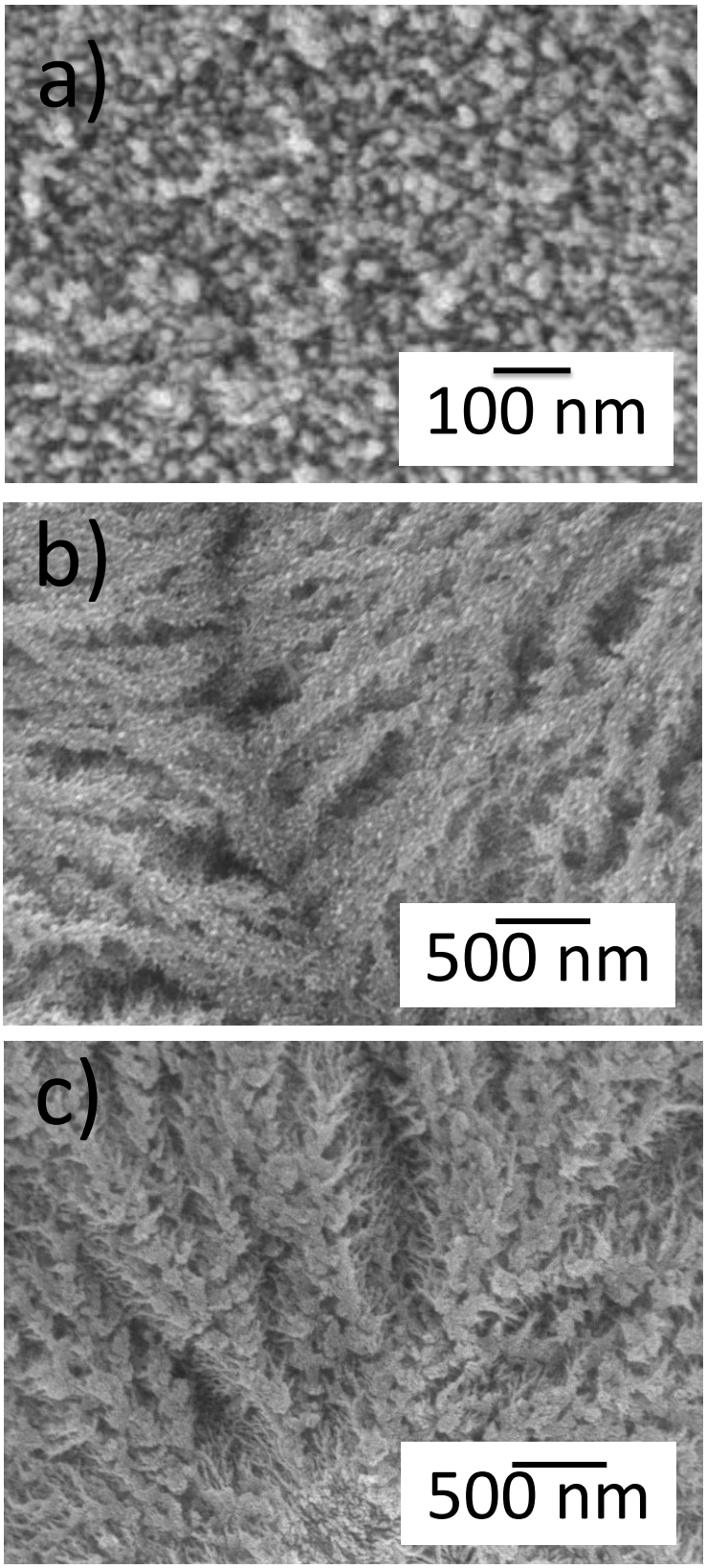

Fig. 3

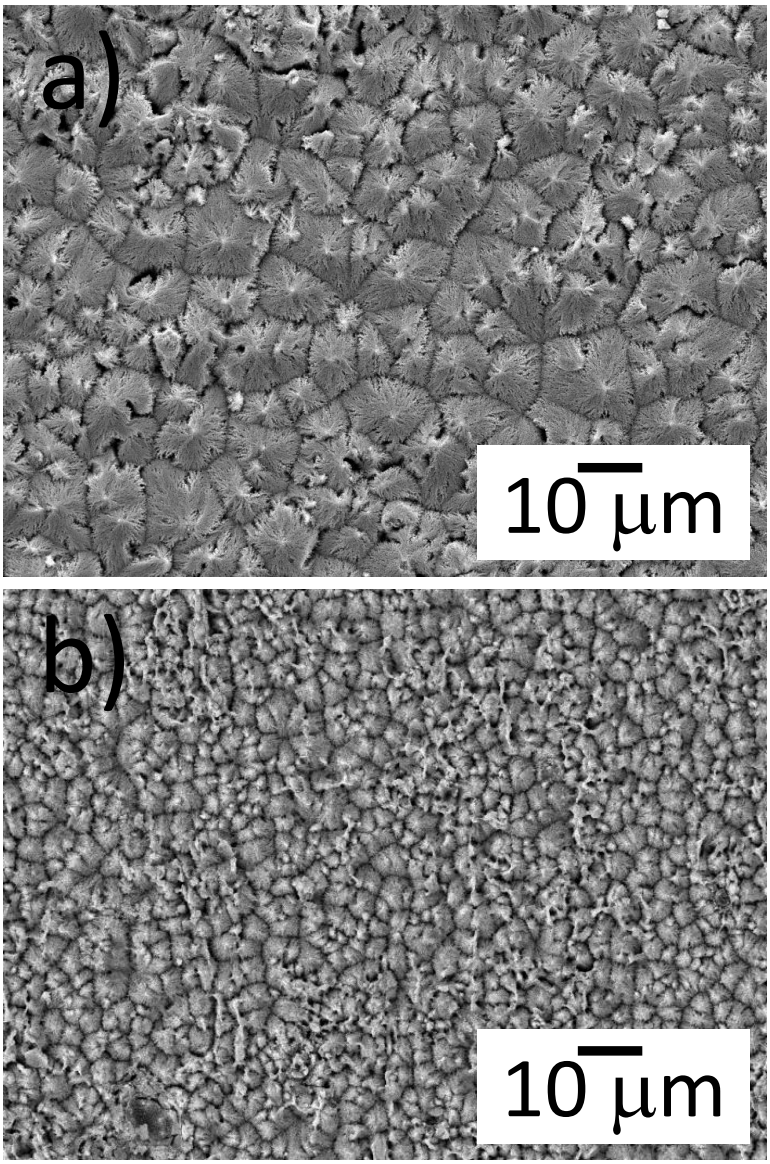

Fig. 4

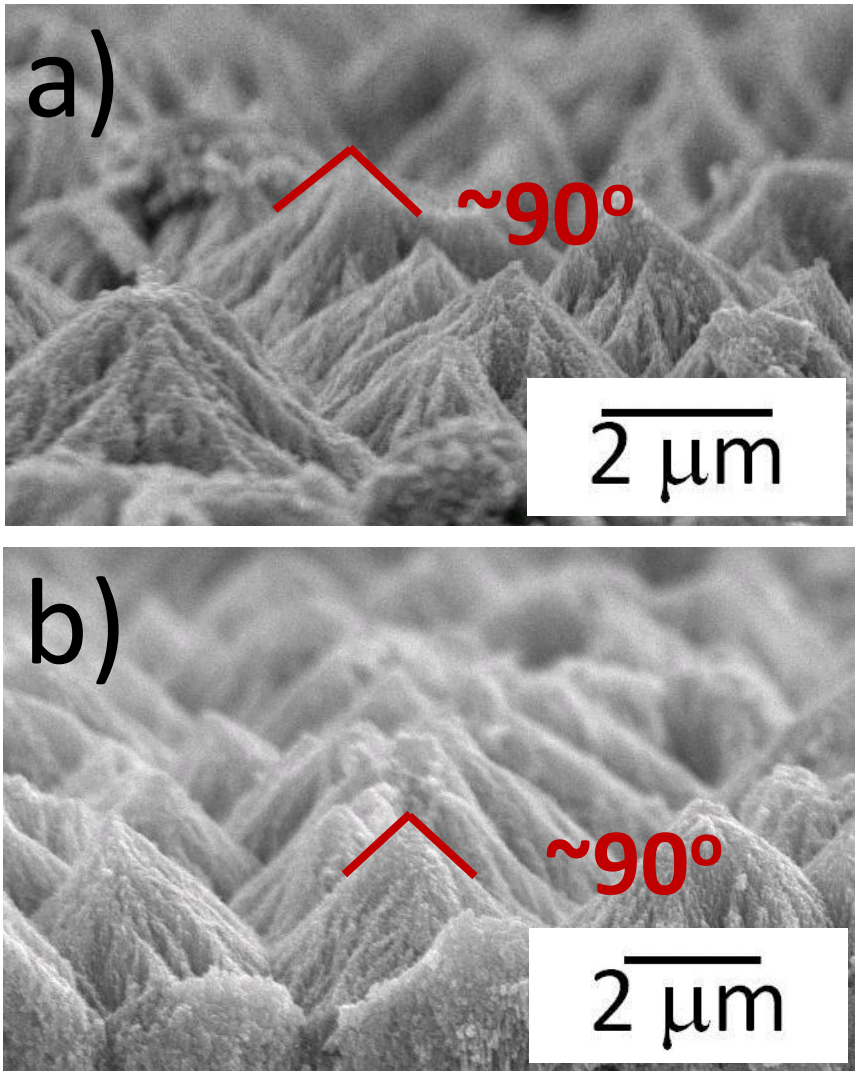

Fig. 5

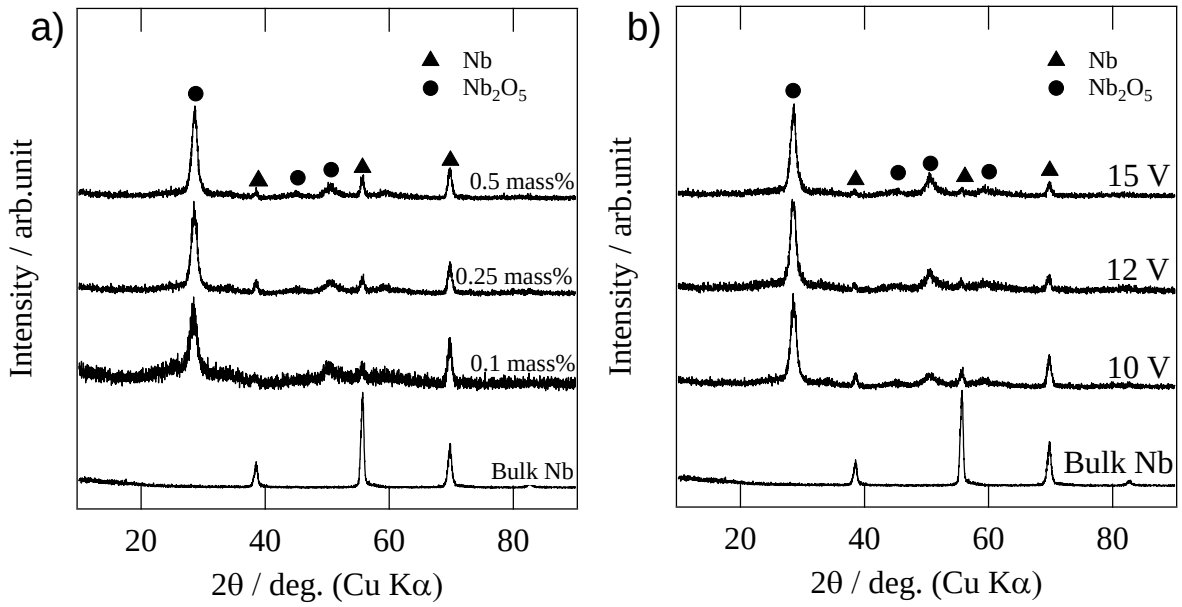
a)
Nb
Nb2O5
0.5 mass%
0.25 mass%
0,1 mass%
Bulk Nb
Intensity / arb.unit
20
40
60
80
2θ / deg. (Cu Kα)
b)
Nb
Nb2O5
15 V
12 V
10 V
Bulk Nb
Intensity / arb.unit
20
40
60
80
2θ / deg. (Cu Kα)

Fig. 6

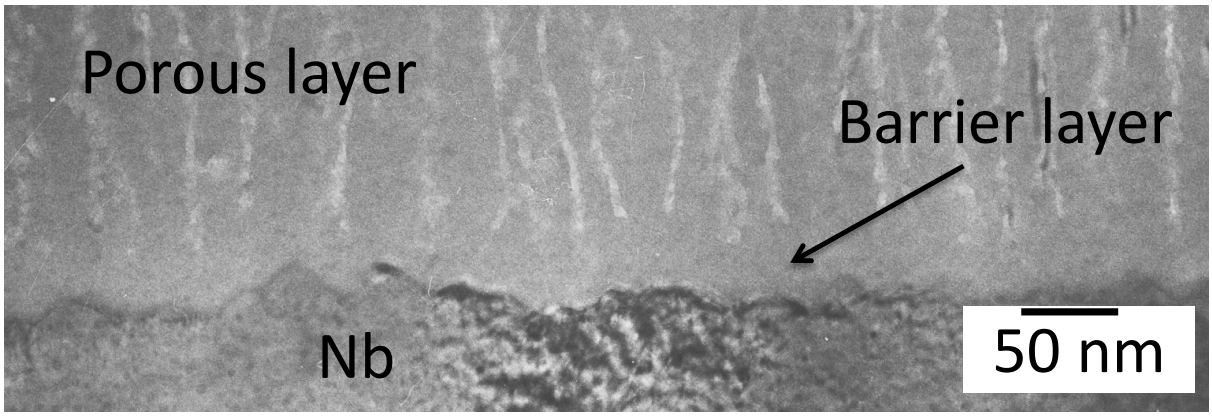

Fig. 7

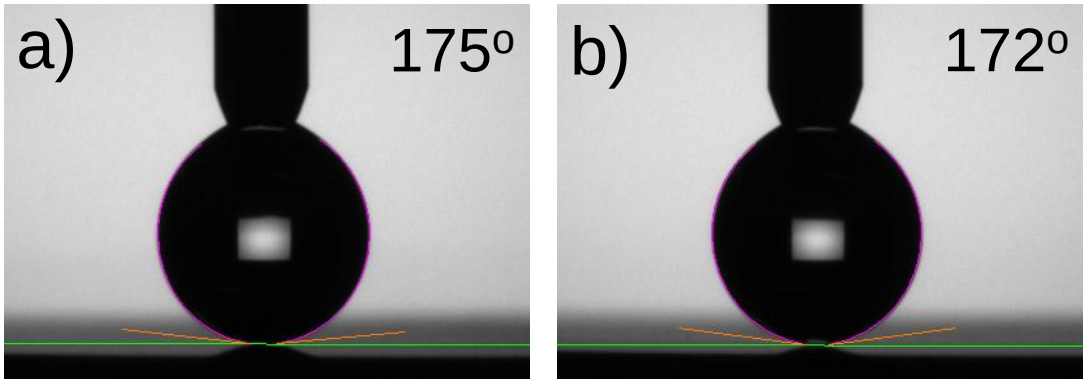

Fig. 8

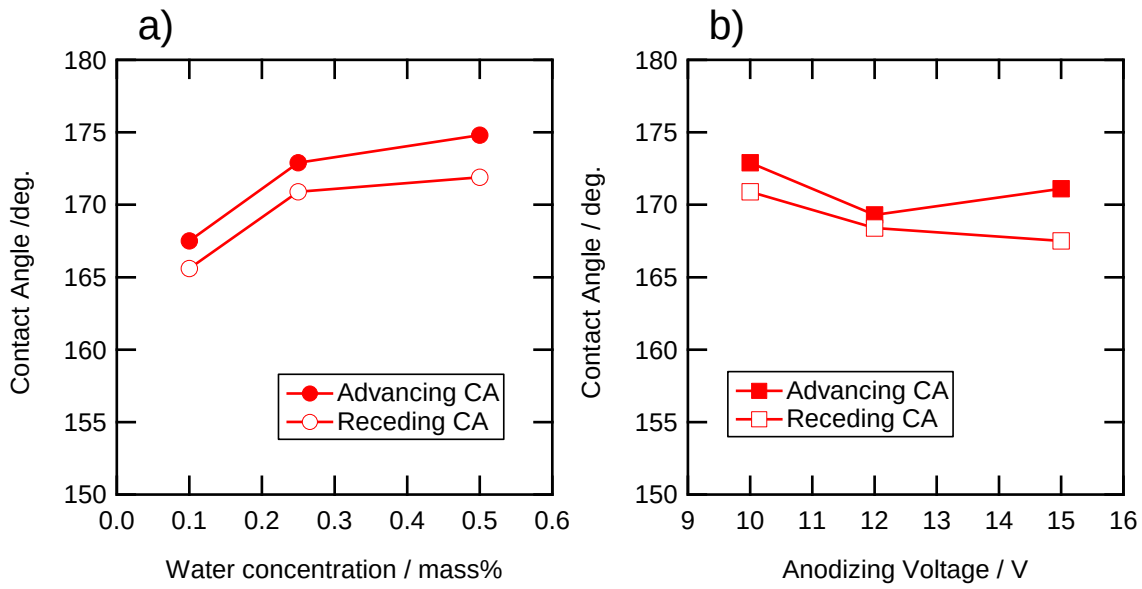
a)
b)
Contact Angle /deg.
Contact Angle / deg.
Water concentration / mass%
Anodizing Voltage / V
Advancing CA
Receding CA
Advancing CA
Receding CA
180
175
170
165
160
155
150
0.0
0.1
0.2
0.3
0.4
0.5
0.6
9
10
11
12
13
14
15
16

Fig. 9

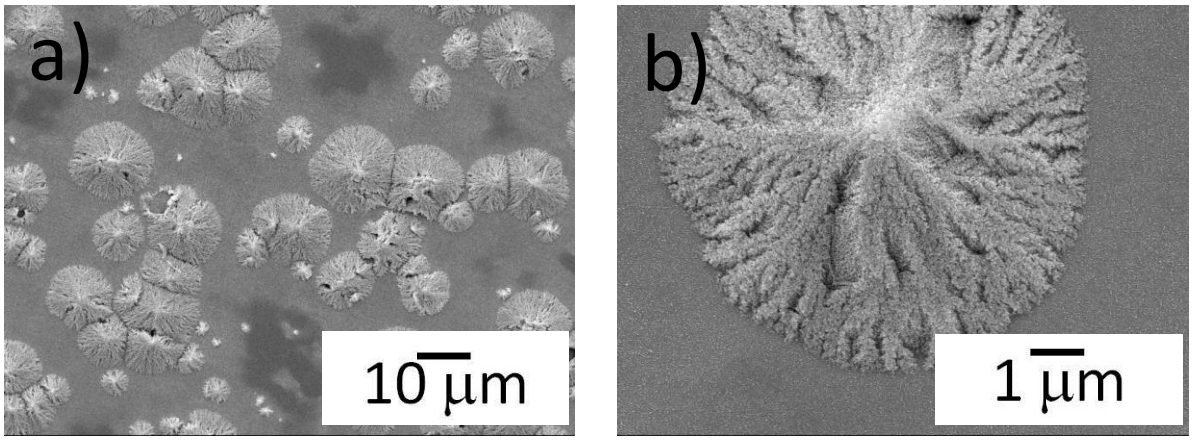

Fig. 10

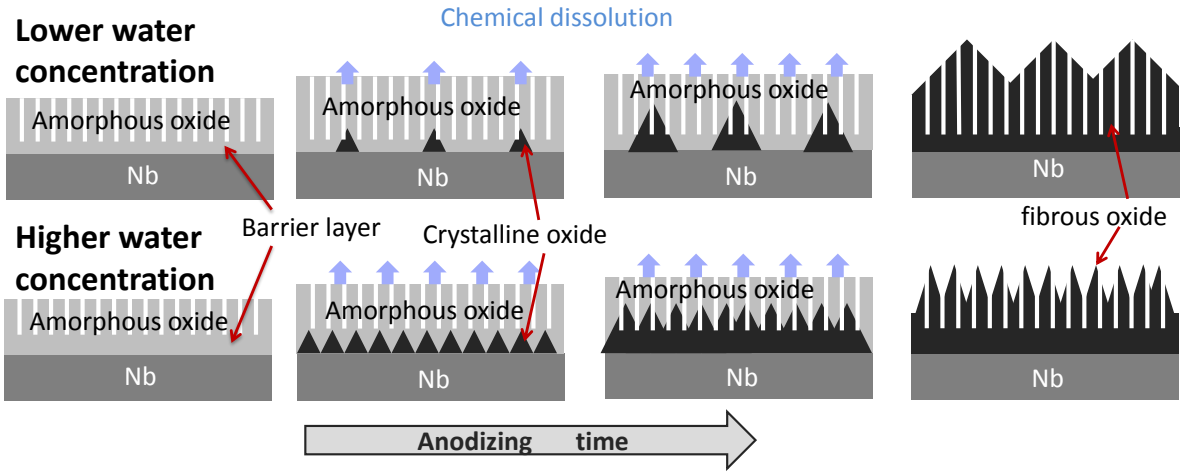
Chemical dissolution
Lower water concentration
Amorphous oxide
Nb
Amorphous oxide
Nb
Amorphous oxide
Nb
Nb
fibrous oxide
Barrier layer
Crystalline oxide
Higher water concentration
Amorphous oxide
Nb
Amorphous oxide
Nb
Amorphous oxide
Nb
Nb
Anodizing time

Fig. 11